NASA TECHNICAL NOTE

HEAT TRANSFER TO A DELTA-WING-HALF-CONE COMBINATION AT MACH NUMBERS OF 7 AND 10

by James C. Dunavant

Langley Research Center
Langley Station, Hampton, Va.

NATIONAL AERONAUTICS AND SPACE ADMINISTRATION • WASHINGTON, D. C. • MARCH 1964

HEAT TRANSFER TO A DELTA-WING—HALF-CONE COMBINATION AT MACH NUMBERS OF 7 AND 10

By James C. Dunavant

Langley Research Center
Langley Station, Hampton, Va.

NATIONAL AERONAUTICS AND SPACE ADMINISTRATION

For sale by the Office of Technical Services, Department of Commerce,
Washington, D.C. 20230 -- Price $1.00

HEAT TRANSFER TO A DELTA-WING—HALF-CONE COMBINATION AT MACH NUMBERS OF 7 AND 10

By James C. Dunavant

SUMMARY

An investigation has been conducted on a delta-wing—half-cone combination at Mach numbers of 7 and 10 through an approximate angle-of-attack range from -5° to 30°. The results of this investigation showed no effect of any shock from the cone on the wing surface pressures or heat transfer. The heat transfer to the stagnation line of the cone is little affected by the presence of the wing. The heat transfer to the wing surface showed agreement with the appropriate laminar or turbulent theory using measured pressures and based on a strip type of flow from the leading edge. Transition, which may be the result of the vortex near the corner, was observed at Reynolds numbers of less than 0.5×10^6.

INTRODUCTION

At various times, consideration has been given to a delta wing with a body on the underside for a hypersonic glide and reentry vehicle. (For example, see refs. 1 and 2.) First estimates of the performance and heating characteristics of such a combination were obtained with the body assumed to be in a uniform flow generated by the delta wing. The delta-wing flow field was in turn modified for the disturbance caused by the body. Previous experimental results however, have failed to show a sharp pressure rise on the delta-wing surface as would be expected due to the shock generated by the body. Furthermore, boundary-layer-induced pressure on a highly swept delta wing (a pressure gradient nearly normal to the local flow direction) produces some strong effects on heat transfer as shown in references 3 and 4. The present experimental investigation was undertaken to study the flow field and heat transfer to a delta wing with a body underneath.

For the present investigation an idealized wing-body combination was selected which consisted of a sharp-edge, 75° swept delta wing and a half-cone having a 5° half-angle. The vertex of the wing and the cone were made to coincide. The corner juncture between the flat wing and cone surface was recognized as a flow-field and heat-transfer problem area since it is the boundary between the dissimilar flows over the cone and flat wing. This area was carefully instrumented to measure the heating. This configuration was tested at free-stream Mach numbers of 6.6, 6.8, and 9.6 with Reynolds numbers, based on model length, of 0.6×10^6, 3.1×10^6, and 1.1×10^6, respectively. Heat transfer and pressure distributions were obtained at angles of attack from -5° to 30°. Oil-flow studies were made to determine boundary-layer flow direction.

SYMBOLS

a_t	speed of sound at stagnation conditions
c	root chord
c_p	specific heat of gas at constant pressure
c_w	specific heat of skin material at wall temperature
D	diameter
h	heat-transfer coefficient, $q/(T_{aw} - T_w)$
K	thermal conductivity of air
k_w	thermal conductivity of skin material
M	free-stream Mach number unless otherwise noted
N_{Pr}	Prandtl number
N_{St}	Stanton number based on free-stream conditions unless otherwise noted
p	static pressure
q	rate of heat flow per unit area
R	Reynolds number based on free-stream conditions unless otherwise noted
r	radius of heat transfer surface
s	surface distance from plane of symmetry (fig. 1)
s_o	reference surface length, distance from plane of symmetry to leading edge
T	absolute temperature
T_{aw}	adiabatic wall temperature
t	time
u	velocity
x	distance from apex parallel to model center line
α	angle of attack of delta-wing flat surface

γ ratio of specific heats

θ angle of ray on cone surface (fig. 1)

Λ sweep angle

λ wall thickness

λ_e effective wall thickness

μ dynamic viscosity

ρ density

ϕ angle of ray on wing surface (fig. 1)

Subscripts:

c based on model length

l local

t total

w wall

x based on length from apex to station, measured parallel to chord

σ conditions behind normal shock

∞ free stream

Superscript:

' denotes parameter evaluated at reference-temperature conditions

APPARATUS AND METHODS

Tunnel and Nozzles

The tests were performed in the nominal Mach 7 and Mach 10 nozzles of the Langley 11-inch hypersonic tunnel. This tunnel is a blowdown facility with a running time of 1 to 2 minutes. Air was preheated to approximately 1160° R for the $M \approx 7$ tests and to 1660° R for the $M \approx 10$ tests. The Mach 7 nozzle, a two-dimensional contoured configuration, has a measured Mach number of 6.6 at a Reynolds number per inch of 0.06×10^6 and a measured Mach number of 6.8 at a Reynolds number per inch of 0.3×10^6. The Mach 10 nozzle, designed from axisymmetrical characteristics, has a square throat and test

section and a measured Mach number of 9.6 at a Reynolds number per inch of 0.1×10^6. The tests were made at these Mach number and Reynolds number conditions through an approximate angle-of-attack range from -5° to 30°.

Models

A sketch of the delta-wing—half-cone model is shown in figure 1. Dimensions and pressure orifice and thermocouple locations are indicated. Figure 2 presents photographs of the model. The model was constructed of inconel sheet, 0.050 inch thick on the lower (cone) surface and 0.031 inch thick on the upper surface. The two surfaces were prebent and instrumented; then, they were roll seamwelded together at the leading edge. The bending operation did not permit a sharp corner at the junction of the cone surface and wing surface. This corner had a radius of 0.078 inch at the exterior surface. This small corner radius was neglected in calculating the surface-distance ratios s/s_o. A solid, uninstrumented model constructed for the oil-flow experiments had the cone and the wing machined in two pieces and a sharp corner at the junction of the cone surface and wing surface. The leading edges of both models were sharpened to thicknesses of about 0.002 inch.

Methods

Pressures.- Pressures were recorded on a six-cell aneroid-type recording instrument. Pressures were measured after 60 seconds of running time to insure that the instrument was fully stabilized. Differential heating on the upper and lower surfaces on the model caused a slight bending of the model, which was observed near the vertex in the schlieren photographs. This bending, which was most obvious at high angles of attack, was observed to increase with running time. At 2 seconds after start of the flow, when the heat transfer was measured, this bending could not be seen and at 60 seconds was small but nevertheless may have some effect on the pressures near the vertex.

Flow visualization.- In addition to side-view schlieren photographs, flow-visualization studies were made with the model spotted with very small drops of a heavy oil and lampblack mixture. After a short flow period from 4 to 30 seconds, the model was removed from the tunnel and the oil streaks which persist after the test were photographed.

Heat transfer.- The heat-transfer data were obtained by using the transient calorimeter technique whereby the rate of heat storage in the model surface was measured locally with the thermocouples attached to the inner surface of the model. The outputs of the thermocouples were recorded on calibrated D'Arsonval type recording galvanometers. The model, initially at room temperature, is positioned in the tunnel before the flow is started. To start the flow, a quick-opening valve was used. Approximately 2 seconds of airflow were required to stabilize settling chamber temperature and pressure, and during this 2-second tunnel transient period the maximum temperature rise at any point on the model surface recorded by the thermocouples was 45° F. However, for about

three-fourths of the recorded data, the temperature rise was less than 20° F. A correction was made to the measured heating rates for heat conducted in the model skin in the spanwise direction, but not in the chordwise direction where the skin temperature gradients were extremely small. The aerodynamic heating rate, including a correction for lateral conduction, is given by

$$q = \lambda_e c_w \rho_w \frac{dT_w}{dt} - k_w \lambda \frac{\partial^2 T_w}{\partial s^2}$$

The derivative of wall temperature with time was determined graphically from the recorded temperature traces. The required second derivative of wall temperature with surface distance was determined from faired wall temperatures by using a three-point finite-differences method. The second derivative at thermocouple location n is given by

$$\left(\frac{\partial^2 T_w}{\partial s^2}\right)_n = \frac{\dfrac{T_{w,n+1} - T_{w,n}}{s_{n+1} - s_n} - \dfrac{T_{w,n} - T_{w,n-1}}{s_n - s_{n-1}}}{\dfrac{s_{n+1} + s_n}{2} - \dfrac{s_n + s_{n-1}}{2}}$$

where the subscripts $n + 1$ and $n - 1$ denote the adjacent thermocouples on either side of thermocouple n.

Where the model surface was flat, the measured skin thickness was used for the effective thickness λ_e. The effective thickness obtained by dividing the volume of the skin by the heated surface area is

$$\lambda_e = \lambda \pm \frac{\lambda^2}{2r} \qquad (1)$$

On the cone the curvature of the skin reduced the effective thickness of the skin from the measured value whereas in the corner it increased the effective thickness. Thermocouples were located approximately at the center of the corner fillet and at the junctures of the corner fillet with the cone and with the wing surface. The relation for λ_e (see eq. (1)) indicates that λ_e changes discontinuously at the juncture of the small corner radius with the cone and the flat wing. Since this discontinuity in effective thickness was unrealistic, the effective thickness of the three corner-fillet thermocouples was arbitrarily set as the average of the measured and the effective thickness. The close spacing of the three thermocouples on the fillet was designed to improve the accuracy of the heating measurement in this region. However, because of the close spacing of the thermocouples, the conduction correction can vary greatly for small temperature differences. It was found that even with fairing of the wall temperatures the conduction correction could not be determined with confidence, and an alternate heating rate was calculated for the corner from the average of the three wall-temperature—time derivatives and a conduction correction based on the average temperature at the three thermocouples.

The heating rates were reduced to a laminar heat-transfer correlating parameter $N_{St}\sqrt{R_x}$ based on free-stream conditions:

$$N_{St}\sqrt{R_x} = \frac{q/(T_{aw} - T_w)}{\rho_\infty u_\infty c_{p,\infty}}\sqrt{\frac{\rho_\infty u_\infty x}{\mu_\infty}}$$

RESULTS AND DISCUSSION

Flow Field

Schlieren photographs.- Schlieren photographs taken of the side view of the model at $M = 6.8$ are shown in figure 3. The results seen are typical of the results at other Mach numbers. Only a single shock is seen to stand out from the lower surface. For this Mach number and at angles of attack above 10°, the shock was located from $2\frac{1}{2}^\circ$ to $3\frac{1}{2}^\circ$ away from the surface of the 5° half-angle cone. In reference 5, tests of a sharp-edge delta wing without the cone placed the shock 4° to 5° from the wing surface. In some unpublished tests of an isolated 5° half-angle cone at this Mach number, the shock was located at an almost constant angle of 2° from the cone surface at the same angles of attack. Theory indicates that a shock would be located more than 7° away from the cone surface if the cone were at zero angle of attack and at a Mach number equal to the local Mach number on the delta wing at $\alpha > 10^\circ$. Thus, the nearness of the shock on the delta-wing—cone model to the position of a shock for an isolated cone is an indication that the delta wing has only a small effect on the flow field of the windward portion of the cone.

Surface oil-flow patterns.- Surface oil-flow patterns on the cone side of the wing are shown for Mach numbers of 6.6, 6.8, and 9.6 in figures 4, 5, and 6, respectively. The oil streaks are generally more indicative of the flow direction of the innermost layer of the boundary layer and thus some idea of the boundary-layer shear and thickness can be gained from interpretation of the length of the streaks of oil in individual tests. For instance, on the average, the streaks were longer near the leading edge than near the trailing edge where the boundary layer is thickest. Comparison of the length of the streaks can be made on any individual test; however, comparison of lengths between different tests cannot be made because of the differences in the running times of the tests. For example, at low angles of attack some oil dots failed to move during test times of 30 seconds or more whereas at high angles of attack some tests were terminated after as little as 4 seconds of flow since the flow pattern was well established.

Careful examination of the photographs and flow patterns on the model failed to show evidence of flow reversal under a separated region at any of the test conditions. A large and unexpected region of very little flow was observed in the boundary layer at the center of the cone at low angles of attack, $\alpha = -5^\circ$ and $\alpha = 0^\circ$. Also, little or no flow exists on the wing surface away from the leading edge. The relatively low shear regions may be a result of an accumulation of low-energy boundary-layer air as found in reference 3 at the

center of a flat, sharp-edge, delta wing. This phenomenon was shown in reference 3 to be highly Mach number dependent, a result that cannot be observed here due to the small Mach number range of the present tests and to the more complicated nature of this model.

Higher angles of attack produced a flow at the center of the cone which can be described as a stagnation line with the oil streaks diverging to either side. Although the streaks on the cone consistently move toward the wing-cone juncture, no streaks are observed to cross onto the wing; they either diminish in length until there is little or no flow or they run parallel to the juncture line giving the effect of a conical flow in the corner region. In all three tests at $\alpha = -5^\circ$, the oil streaks along a ray on the cone surface about midway between the center of the cone and the wing surface showed a region of higher shear than surrounding regions. Usually these streaks tend to diverge but at times are seen to converge or cross. This change suggests that one or more vortices may exist near the corner along radial lines from the vertex. At higher angles of attack similar flow patterns occur but are less distinct. (For example, see the photographs at $\alpha = 5^\circ$ and $\alpha = 25^\circ$ in fig. 4.)

Several of the photographs clearly show that transition is occurring in the corner region. The photographs at $\alpha = 20^\circ$ for $M = 6.6$ and $M = 9.6$ (figs. 4 and 6) show a region of little or no flow near the corner about mid-length of the model; that is, aft of the forward region which is subject to high laminar shear. Over the rear half of the model the flow or shear near the model corner surface greatly increases. This condition can be conveniently explained by transition from the low-energy laminar boundary layer to a turbulent boundary layer having much higher shear at the surface. To a lesser degree this phenomenon can be seen at other angles of attack at Mach numbers of 6.6 and 9.6; however, in the Mach number 6.8 tests (fig. 5), which had a Reynolds number much greater than in the other tests, no low shear region over the forward portion of the model was observed.

Pressures.- The ratio of measured to free-stream static pressure is plotted against the spanwise-surface-distance ratio in figure 7. The spanwise distributions show constant pressure over the cone near zero angle of attack, and the value is only slightly greater than that on the wing surface. At the high angles of attack the pressure, as expected, is a maximum on the cone at the center of the model, decreases toward the corner, and is relatively uniform over the wing surface. At no condition do the pressures on the wing surface clearly indicate any pressure rise that might be associated with a cone shock impinging on the wing surface. As in reference 2, the pressure on the wing surface near the cone at $\alpha = 0^\circ$ is shown to be approximately equal to the sum of the cone-flow-field pressure plus the wing-boundary-layer displacement pressure.

At $M = 6.8$ the pressure distributions shown were obtained at a Reynolds number of 3.1×10^6 for angles of attack up to 22.2°; the pressures at the two higher angles of attack could be obtained only at a lower Reynolds number of 0.6×10^6. (See fig. 7(a).) Thus, the abrupt change in pressure distribution and in the variation of pressure with angle of attack occurs with a simultaneous change in Reynolds number. Theory which assumes the pressure to be determined

largely by the inviscid flow field, hence independent of Reynolds number, also indicates a continuous change in distribution and pressure level with angle of attack; the abrupt change has not been explained.

Heat transfer.- Spanwise distributions of the laminar heat-transfer correlating parameter $N_{St}\sqrt{R_x}$ at the various angles of attack are plotted for the forward thermocouple station in figures 8(a), 9(a), and 10(a) at Mach numbers of 6.6, 6.8, and 9.6, respectively. Similar distributions for the rearmost thermocouple station are plotted in figures 8(b), 9(b), and 10(b). Distributions of heating at approximately zero angle of attack are compared with theoretical distributions for the three Mach number and Reynolds number conditions in figure 11. Heat-transfer correlating-parameter data plotted against angle of attack are compared with the results calculated from laminar theory for the center of the model (stagnation line on the cone) in figure 12, and for those from laminar and turbulent strip theories for the 6°, 8°, and 10° rays on the wing surface in figure 13. The equations for the laminar and turbulent theories used in the presentation of figures 11 to 13 are given in the appendix. The measured pressures are used in the strip theory.

At low angles of attack the measured stagnation-line heating agrees well with laminar conical-flow strip theory (fig. 12). At the higher angles of attack the data fall between the results for the conical-flow and the cross-flow theories. In reference 6, a similar result is shown for a body alone at comparable angles of attack. These results are to be expected in view of the flow patterns seen in figures 4, 5, and 6, which show the oil streaks to diverge from a conical flow increasingly at angles of attack above 10°.

The heating distribution and level on the cone at $\alpha \approx 0^\circ$ and low Reynolds number agrees well with theory for the isolated cone as shown in figure 11(a). However, at higher Reynolds number and particularly for the rearward station, the deviations from the theory are considerable. Large differences between the experimental and theoretical results also are shown at $M = 9.6$ in figure 11(c). At the higher angles of attack (see figs. 8 to 10), the heating always shows an initially decreasing trend with distance from the center line; this decrease, in many cases, continues almost to the corner region. The distributions shown are indicative of a cross flow at high angles of attack and of a conical flow at low angles of attack on the cone stagnation line and adjacent region. The distributions, as well as the similarity of the variation of stagnation-line heating with angle of attack (fig. 12) with the heating variation for a body alone (ref. 6), lead one to conclude that the heat transfer to the windward part of the cone is little affected by the presence of the wing.

The distribution of heating on the wing surface at $\alpha \approx 0^\circ$ is compared in figure 11 to that calculated from a laminar theory for a strip type of flow. At Mach numbers of 6.6 and 9.6, the experimental data indicate that the heating over much of the wing surface is lower than that derived from theory and tends to rise toward the leading edge. P. Calvin Stainback of the Langley Research Center obtained some heat-transfer test results for a sharp-edge corner alined with the flow (presented in fig. 52-13 of ref. 4) which showed a trend, particularly at the lower Reynolds numbers, of decreased heat transfer from the Mach wave position to the corner. Thus, the less-than-theory heating measured here

appears to be a typical characteristic of corner flow. A like comparison at $R_c = 3.1 \times 10^6$, $M = 6.8$, and $\alpha \approx 0^\circ$ does not exist, but this particular test does not conform to the general trend of heating results shown in figure 9.

Unlike the measured heating over the windward part of the cone, the laminar heat-transfer correlating parameter $N_{St}\sqrt{R_x}$ does not correlate the measured heating on much of the wing surface and in the corner region. Figures 8 and 9 give spanwise distributions of the laminar heat-transfer correlating parameter for Reynolds numbers from 0.3×10^6 to 2.8×10^6. At high angles of attack, the value of $N_{St}\sqrt{R_x}$ increases by as much as a factor of 3 at one angle of attack with the increase in Reynolds number. Comparison of measured heating with a laminar and turbulent strip theory on the wing surface at ray locations $\phi = 6^\circ$, $\phi = 8^\circ$, and $\phi = 10^\circ$ is made in figure 13. At the lower Reynolds number and at $M \approx 7$ (fig. 13(a)), the measured values agree well with the laminar theory on the two rays nearest the leading edge, $\phi = 8^\circ$ and $\phi = 10^\circ$. The heating near the corner, $\phi = 6^\circ$, at the rearward station tends toward the turbulent theory value. At the higher Reynolds number (fig. 13(b)), the measured heating closely follows the theoretical turbulent heating even though the assumption of stripwise flow used in calculating the theoretical heating is not entirely in accord with the flow pattern observed in the oil-flow test. A similar comparison of heating for the tests at $M = 9.6$ in figure 13(c) indicates that many of the measured heating-rate values at the rearward station at high angles of attack are in agreement with the theoretical turbulent values and that the heating for the forward station is between the laminar and turbulent rates. The agreement of the trends of the measured heating rates with the laminar and turbulent theory, along with the evidence of transition observed in the oil-flow tests, indicates that transition and turbulent flow are being obtained at very low Reynolds numbers, less than 0.5×10^6 at some conditions. This transition which first occurs on the ray nearest the corner, $\phi = 6^\circ$, must be associated with corner flow. The experimental results here do not clearly define the flow in the corner, although as previously discussed there is some evidence in the oil-flow photographs of a vortex in the corner and it may be the cause of the early transition obtained in the tests.

SUMMARY OF RESULTS

The pressure, heat-transfer, and surface-oil-streak investigation of the delta-wing half-cone configuration has indicated the following results:

1. No local pressure change which would indicate shock—boundary-layer interactions to be present was observed on the model surface.

2. The oil-streak tests at low angles of attack showed a region of low shear in the corner before transition. Some evidence of a vortex near the corner was also seen.

3. The heat transfer to the stagnation line of the cone is little affected by the presence of the wing and is in fair agreement with the appropriate laminar strip-flow or cross-flow theory for a cone alone.

4. The heat transfer to the wing surface showed agreement with the appropriate laminar or turbulent theory using measured pressures and based on a strip type of flow from the leading edge. At low angles of attack and before transition occurs, a region of low shear and heat transfer is present on the wing surface adjacent to the corner. Transition, which may be the result of the vortex near the corner, was observed at Reynolds numbers of less than 0.5×10^6.

Langley Research Center,
National Aeronautics and Space Administration,
Langley Station, Hampton, Va., November 18, 1963.

APPENDIX

THEORETICAL EVALUATION OF HEATING OF MODEL

Laminar Strip Theory

The laminar heat-transfer correlating parameter is given by the Blasius skin-friction relationship and Reynolds analogy for a flat plate in terms of local reference-temperature conditions as follows:

$$\left(N'_{St}\sqrt{R'}\right)_l = \frac{0.664}{2\left(N'_{Pr}\right)^{2/3}}$$

The local stream Stanton number and Reynolds number are related to the reference-temperature quantities by

$$N_{St,l} = N'_{St,l}\,\frac{T_l}{T'}$$

$$R_l = R'_l\,\frac{\mu' T'}{\mu_l T_l}$$

Rewriting the laminar flat-plate heat-transfer correlating parameter in terms of free-stream conditions results in

$$N_{St,\infty}\sqrt{R_\infty} = \frac{0.664}{2\left(N'_{Pr}\right)^{2/3}}\,\frac{c_{p,l}}{c_{p,\infty}}\sqrt{\frac{p_l M_l \mu' T_l}{p_\infty M_\infty \mu_l T'}}\left(\frac{T_\infty}{T_l}\right)^{1/4}$$

where the Reynolds number characteristic length is the local streamwise length from the leading edge. For comparison with the data, the heat-transfer correlating parameter with the Reynolds number based on the chordwise length from the apex to the measuring station is

$$N_{St}\sqrt{R_x} = \frac{0.664}{2\left(N'_{Pr}\right)^{2/3}}\,\frac{c_{p,l}}{c_{p,\infty}}\sqrt{\frac{p_l M_l \mu' T_l}{p_\infty M_\infty \mu_\infty T'}}\left(\frac{T_\infty}{T_l}\right)^{1/4}\left(\frac{\cot\Lambda}{\cot\Lambda - \tan\phi}\right)$$

Local conditions of temperature and Mach number were assumed to be the conditions behind a single oblique shock which would raise the free-stream pressure to the measured local pressure. Reference temperature was determined for local flow conditions from Monaghan (ref. 7).

The laminar-strip-theory heating was also compared with the heating at the center of the cone at low angles of attack by using the measured cone pressure and assuming the cone heating to be $\sqrt{3}$ times the flat-plate heating.

Turbulent Strip Theory

Turbulent heating on a flat plate, again in terms of local reference-temperature condition, is (from ref. 8)

$$\left[N'_{St}(R')^{1/5}\right]_l = \frac{0.0592}{2\left(N'_{Pr}\right)^{2/3}}$$

The local turbulent Stanton number is, then,

$$N_{St,l} = \frac{0.0592}{2\left(N'_{Pr}\right)^{2/3}\left(R_l\right)^{1/5}}\left(\frac{T_l}{T'}\right)\left(\frac{\mu' T'}{\mu_l T_l}\right)^{1/5}$$

This local turbulent Stanton number was converted to the form of the laminar heat-transfer correlating parameter for comparison of data. Hence, based on free-stream conditions and the length from the apex to the chordwise station, the turbulent theory is given by

$$N_{St}\sqrt{R_x} = \sqrt{R_x}\,\frac{0.0592}{2\left(N'_{Pr}\right)^{2/3}}\,\frac{\rho_l u_l c_{p,l}}{\rho_\infty u_\infty c_{p,\infty}}\left(\frac{T_l}{T'}\right)^{4/5}\left(\frac{\mu'}{\rho_l u_l}\right)^{1/5}\left[\frac{\cot\Lambda}{x(\cot\Lambda - \tan\phi)}\right]^{1/5}$$

The same assumption of local flow conditions was made as for the laminar theory, and the reference temperature was taken from Monaghan (ref. 9).

Cross-Flow Theory

The heat transfer at the stagnation line of a two-dimensional blunt body is determined, as in reference 5, from

$$h = 0.57 N_{Pr,\sigma}^{0.4}\, K_\sigma \sqrt{\frac{\rho_\sigma}{\mu_\sigma}\frac{du}{ds}}$$

The laminar heat-transfer correlating parameter which results from this equation for the stagnation line is

$$N_{St}\sqrt{R_x} = 0.57 N_{Pr,\sigma}^{-0.6}\,\frac{c_{p,\sigma}}{c_{p,\infty}}\sqrt{\frac{\rho_\sigma \mu_\sigma}{\rho_\infty \mu_\infty}\frac{x}{u_\infty}\frac{du}{ds}}$$

The velocity gradient was evaluated from the data correlation, as in reference 5, and is for a sphere or cylinder

$$\frac{du}{ds} = 2.315 \frac{a_t}{D}$$

The cone was considered to be locally a cylinder swept, with respect to the flow, at an angle equal to the angle of the stagnation line on the cone. As in reference 10, h $\left(\text{and hence } N_{St}\sqrt{R_x}\right)$ was assumed to vary as the cosine of the angle of the sweep of the stagnation line of the cone.

REFERENCES

1. Eggers, A. J., Jr., and Syvertson, Clarence A.: Aircraft Configurations Developing High Lift-Drag Ratios at High Supersonic Speeds. NACA RM A55L05, 1956.

2. McLellan, Charles H., and Ladson, Charles L.: A Summary of the Aerodynamic Performance of Hypersonic Gliders. NASA TM X-237, 1960.

3. Bertram, Mitchel H., and Henderson, Arthur, Jr.: Recent Hypersonic Studies of Wings and Bodies. ARS Jour., vol. 31, no. 8, Aug. 1961, pp. 1129-1139.

4. Bertram, Mitchel H., Fetterman, David E., Jr., and Henry, John R.: The Aerodynamics of Hypersonic Cruising and Boost Vehicles. Proceeding of the NASA-University Conference on the Science and Technology of Space Exploration, Vol. 2, NASA SP-11, 1962, pp. 215-234. (Also available as NASA SP-23.)

5. Dunavant, James C.: Investigation of Heat Transfer and Pressures on Highly Swept Flat and Dihedraled Delta Wings at Mach Numbers of 6.8 and 9.6 and Angles of Attack to 90°. NASA TM X-688, 1962.

6. Feller, William V.: Heat Transfer to Bodies at Angles of Attack. NACA RM L57D19c, 1957.

7. Monaghan, R. J.: An Approximate Solution of the Compressible Laminar Boundary Layer on a Flat Plate. R. & M. No. 2760, British A.R.C., 1956.

8. Schlichting, Hermann (J. Kestin, trans.): Boundary Layer Theory. McGraw-Hill Book Co., Inc., 1955, p. 433.

9. Monaghan, R. J.: On the Behavior of Boundary Layers at Supersonic Speeds. Fifth International Aeronautical Conference (Los Angeles, Calif., June 20-23, 1955), Inst. Aero. Sci., Inc., 1955, pp. 277-315.

10. Feller, William V.: Investigation of Equilibrium Temperatures and Average Laminar Heat-Transfer Coefficients for the Front Half of Swept Circular Cylinders at a Mach Number of 6.9. NACA RM L55F08a, 1955.

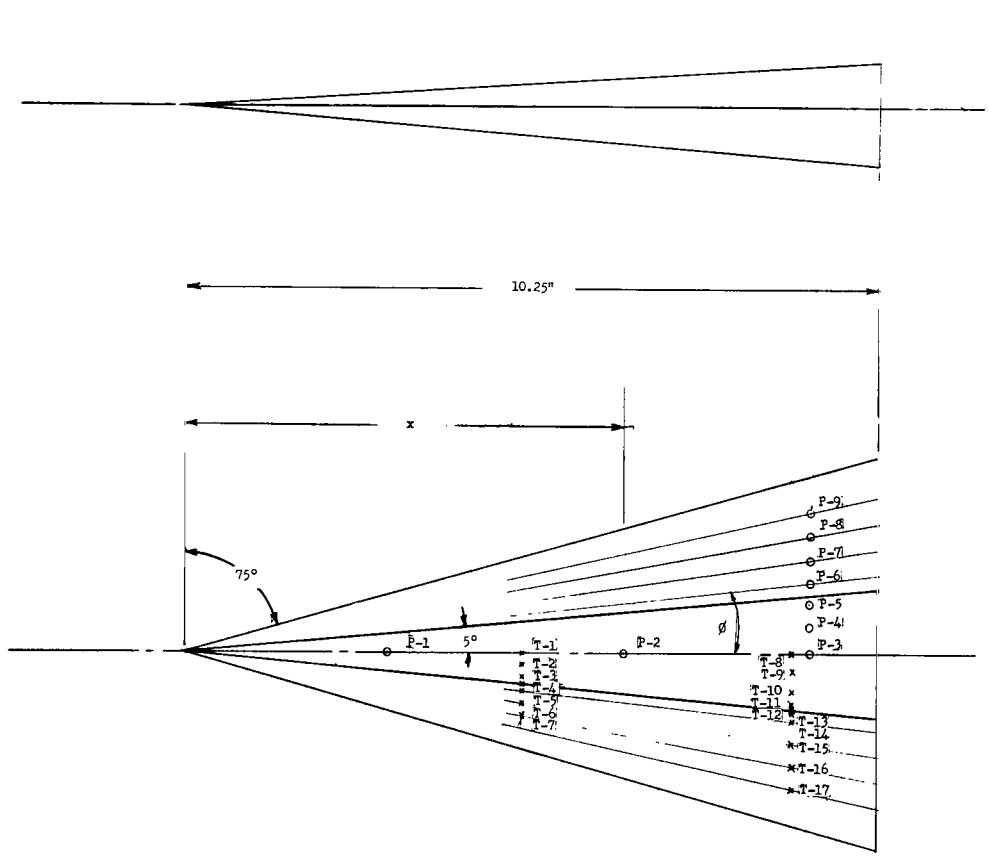

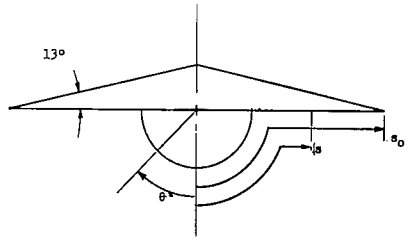

INSTRUMENTATION

Cone

Pressure orifices				Thermocouples			
No.	x, in.	θ, deg	s/s_o	No.	x, in.	θ, deg	s/s_o
P-1	3.00	0	0	T-1	5.00	0	0
P-2	6.50	0	0	T-2	5.00	30	.145
P-3	9.25	0	0	T-3	5.00	60	.286
P-4	9.25	30	.145	T-4	5.00	90	.431
P-5	9.25	60	.286	T-8	9.00	0	0
				T-9	9.00	30	.145
				T-10	9.00	60	.286
				T-11	9.00	81	.389
				T-12	9.00	90	.431

Wing

Pressure orifices				Thermocouples			
No.	x, in.	ø, deg	s/s_o	No.	x, in.	ø, deg	s/s_o
P-6	9.25	6	0.488	T-5	5.00	6	0.488
P-7	9.25	8	.599	T-6	5.00	8	.599
P-8	9.25	10	.712	T-7	5.00	10	.712
P-9	9.25	12	.826	T-13	9.00	5.4	.456
				T-14	9.00	6	.488
				T-15	9.00	8	.599
				T-16	9.00	10	.712
				T-17	9.00	12	.826

Figure 1.- Delta-wing—cone heat-transfer and pressure model.

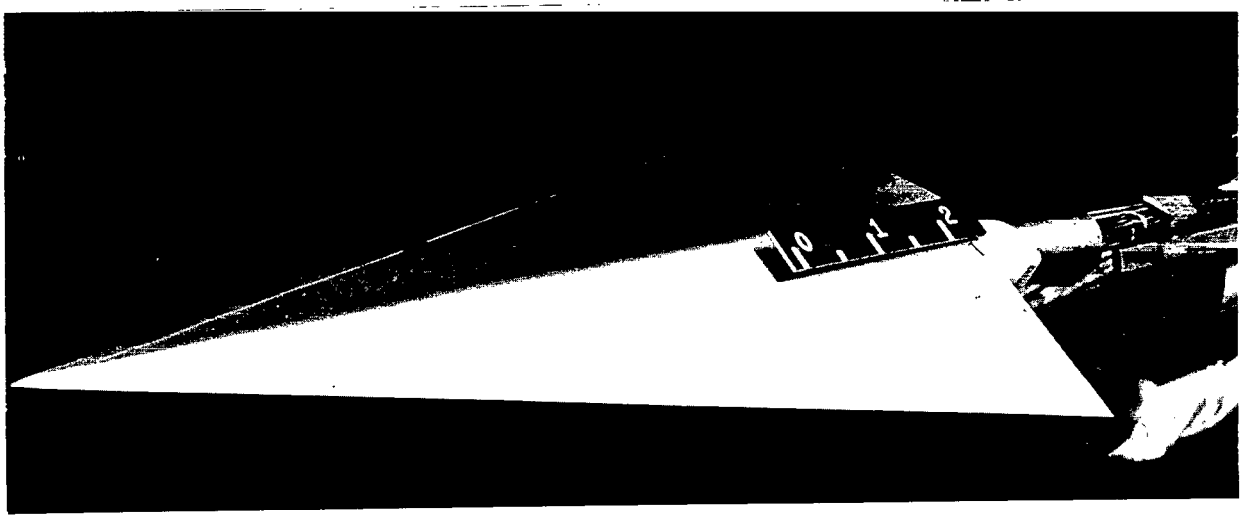

(a) Top.

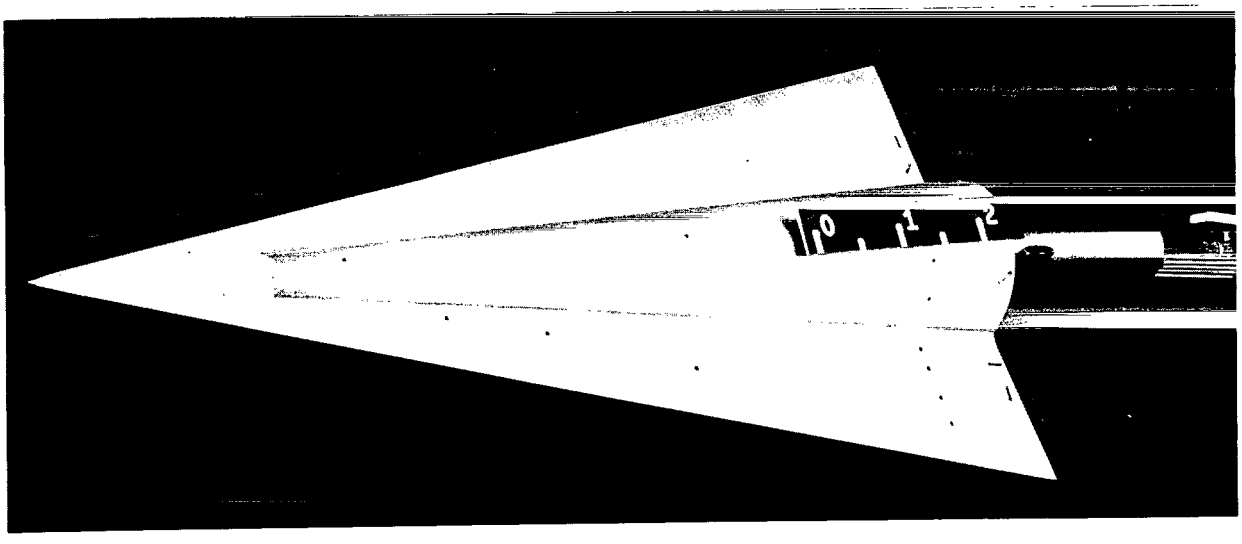

(b) Bottom.

Figure 2.- Photographs of model. L-63-9246

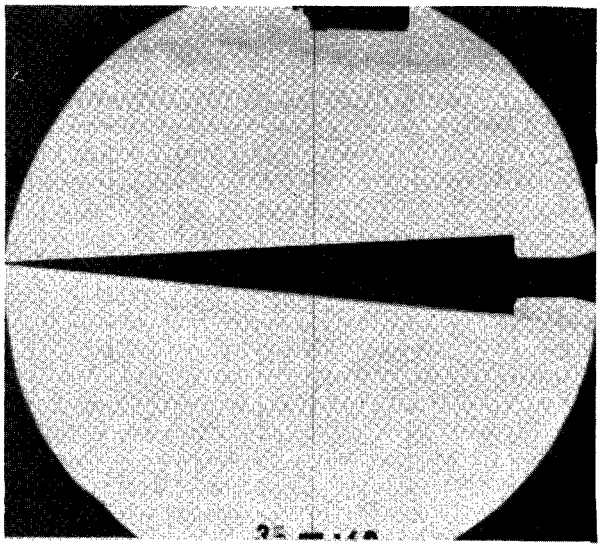

(a) $\alpha = 0.5^{\circ}$.

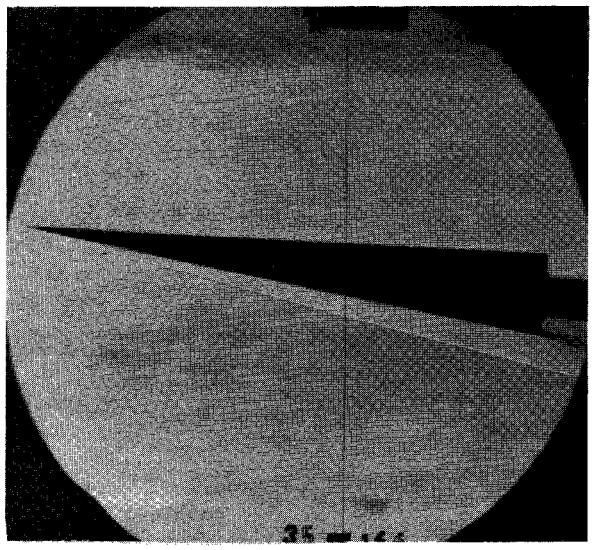

(b) $\alpha = 6.0^{\circ}$.

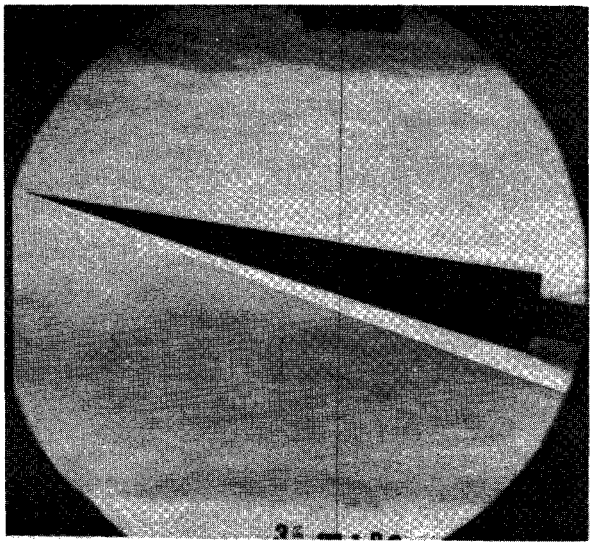

(c) $\alpha = 11.4^{\circ}$.

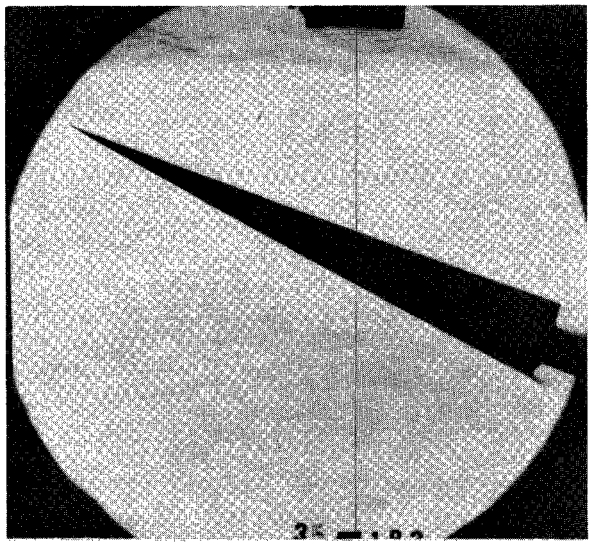

(d) $\alpha = 22.2^{\circ}$.

L-63-9247

Figure 3.- Schlieren photographs of delta-wing—cone model at angles of attack. M = 6.8; $R_c = 3.1 \times 10^6$.

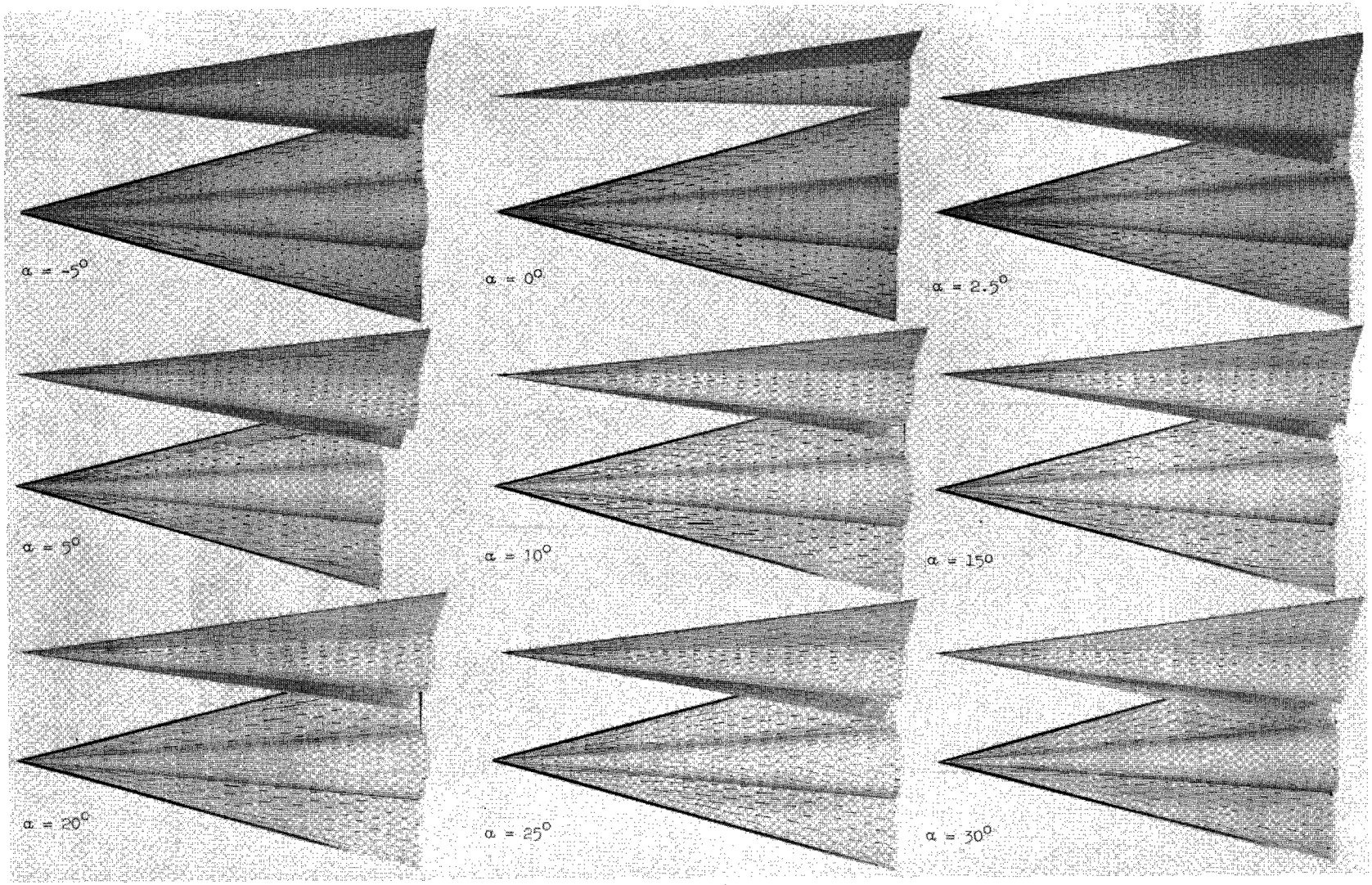

L-63-9248

Figure 4.- Photographs of oil streaks on delta-wing—cone configuration at $M = 6.6$ and $R_c = 0.6 \times 10^6$.

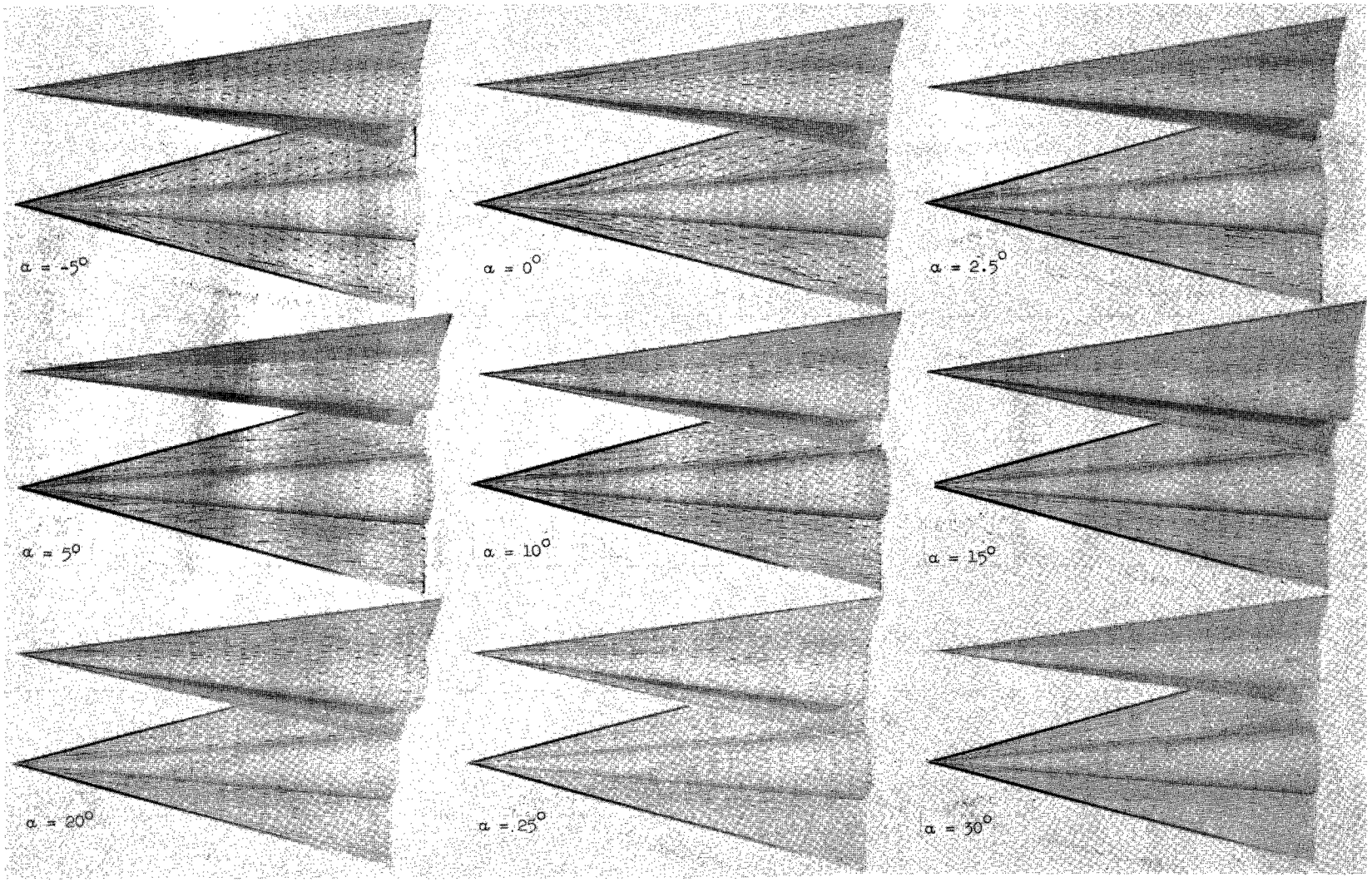

L-63-9249

Figure 5.- Photographs of oil streaks on delta-wing—cone configuration at $M = 6.8$ and $R_c = 3.1 \times 10^6$.

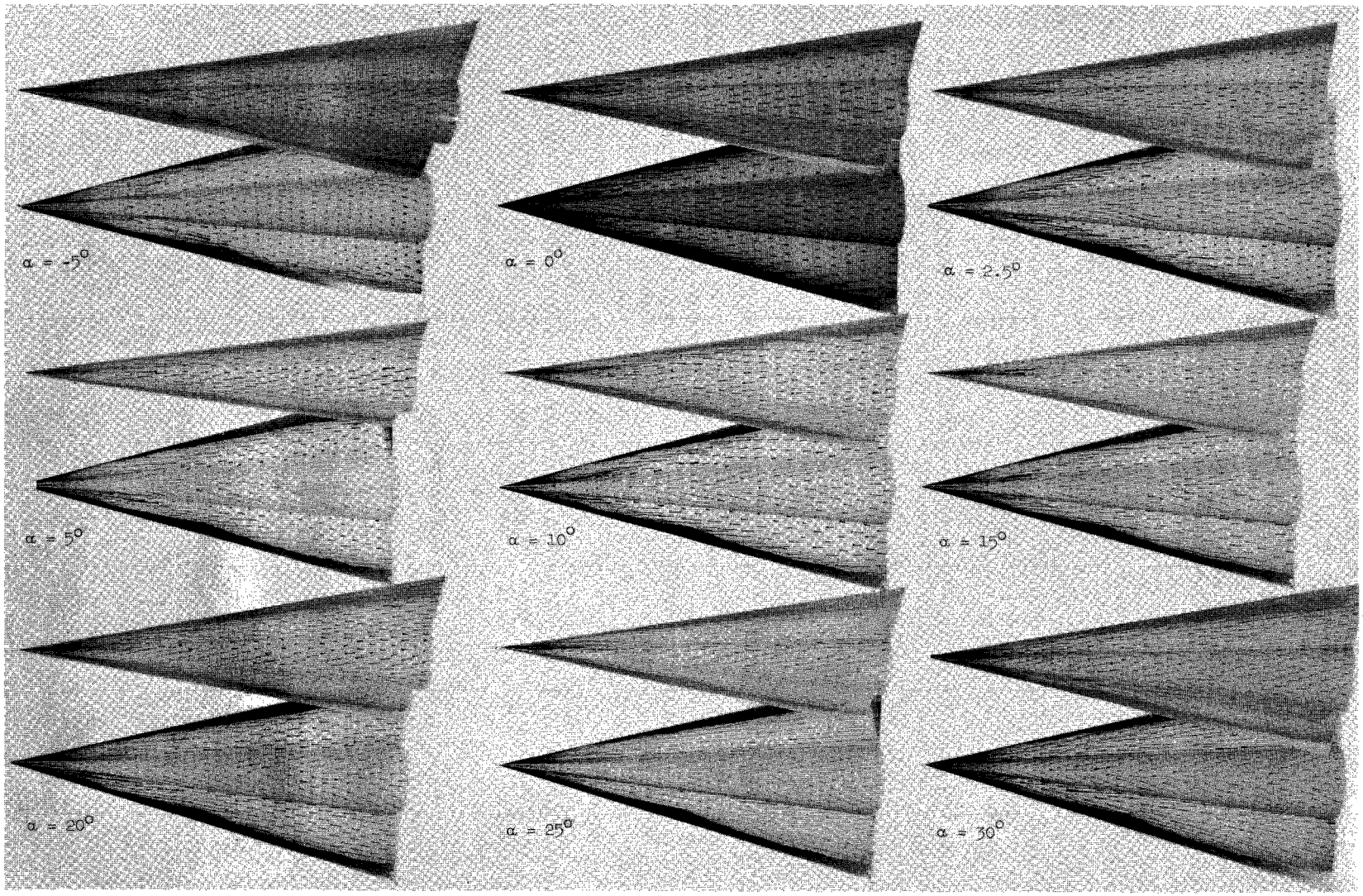

L-63-9250

Figure 6.- Photographs of oil streaks on delta-wing—cone configuration at $M = 9.6$ and $R_c = 0.9 \times 10^6$.

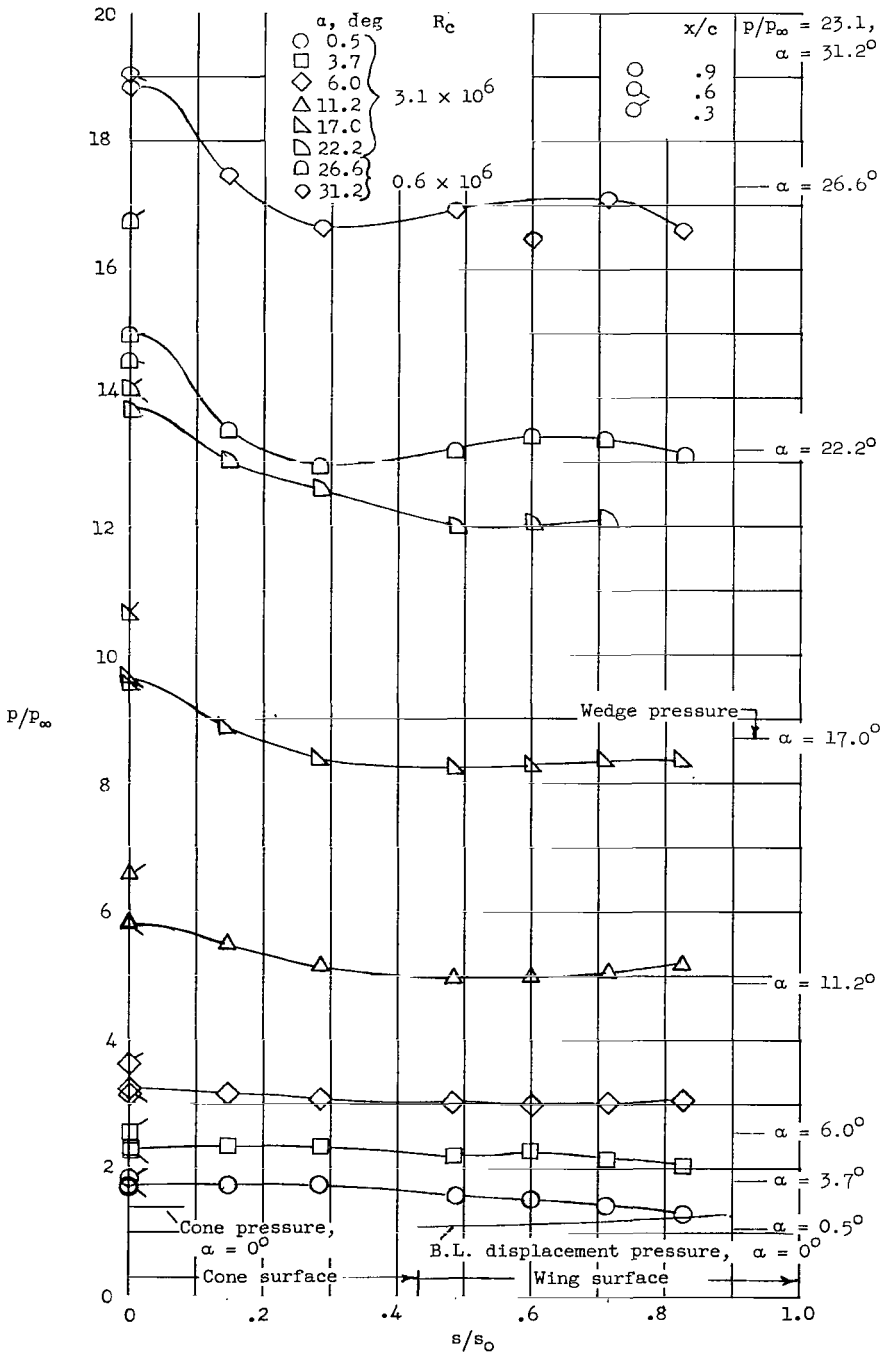

(a) M = 6.8.

Figure 7.- Spanwise pressures on a delta-wing—half-cone configuration.

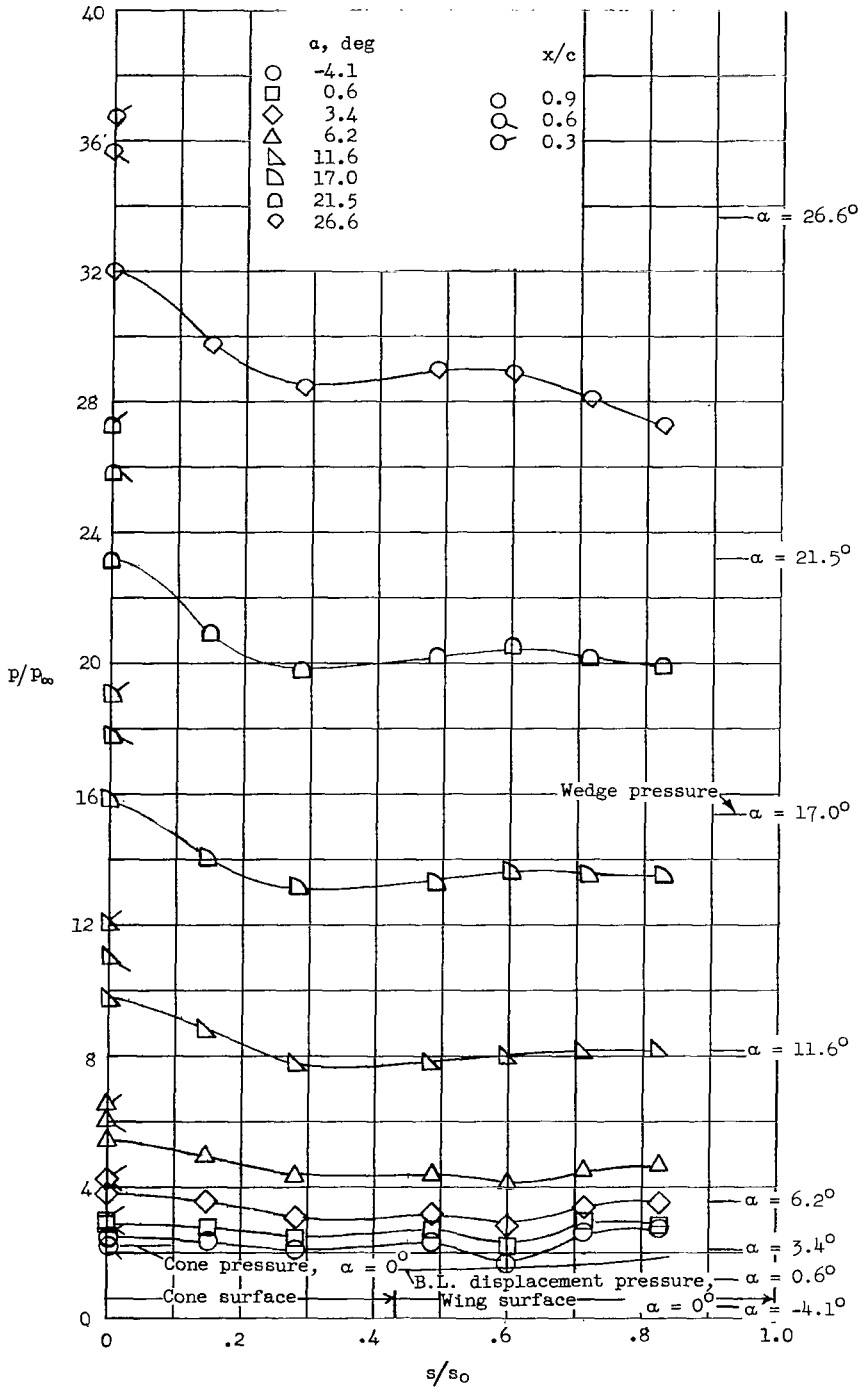

(b) M = 9.6; $R_c = 1.1 \times 10^6$.

Figure 7.- Concluded.

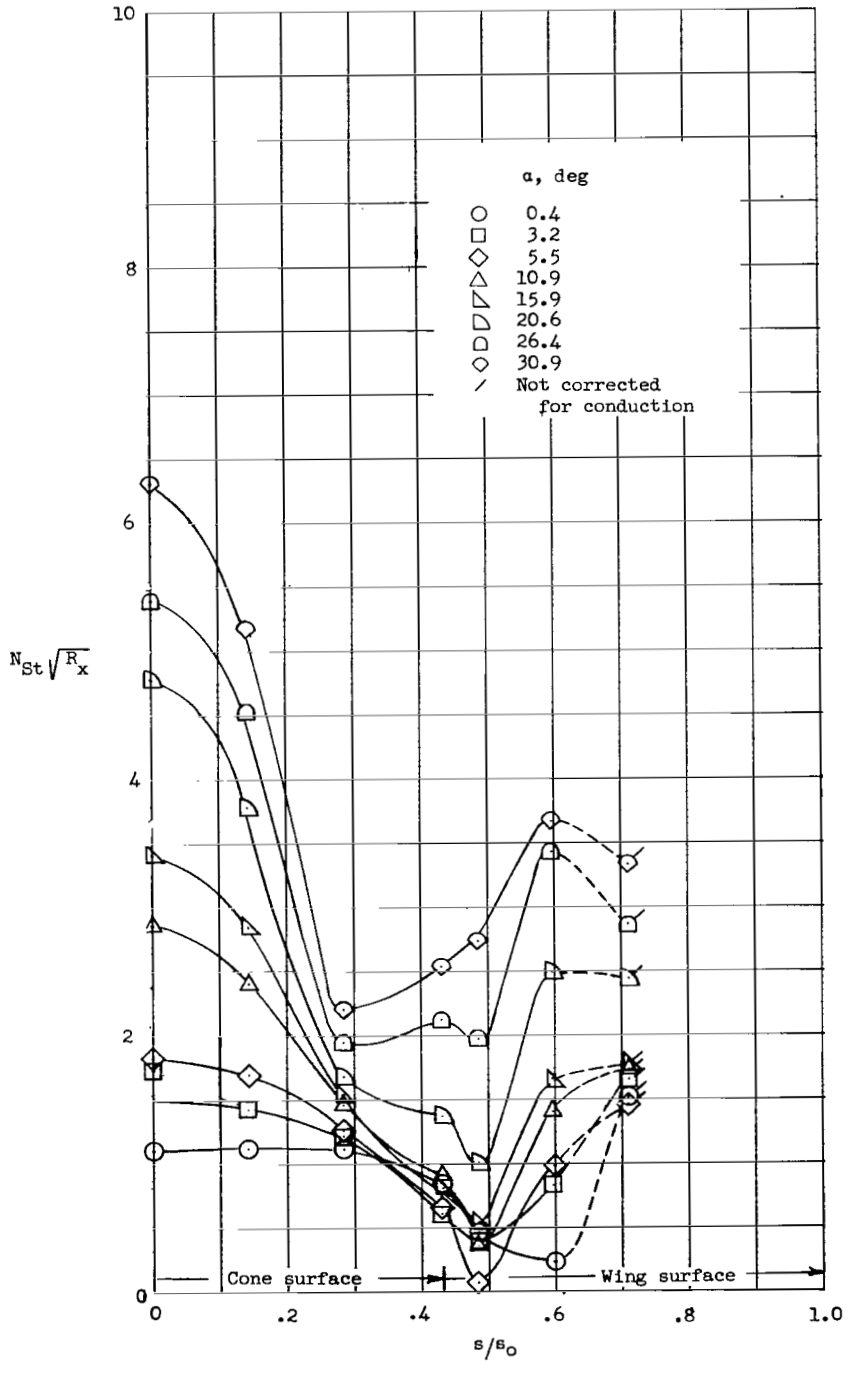

(a) $R_x = 0.3 \times 10^6$.

Figure 8.- Spanwise heating distribution on a delta-wing—half-cone configuration at $M = 6.6$ and $R_c = 0.3 \times 10^6$.

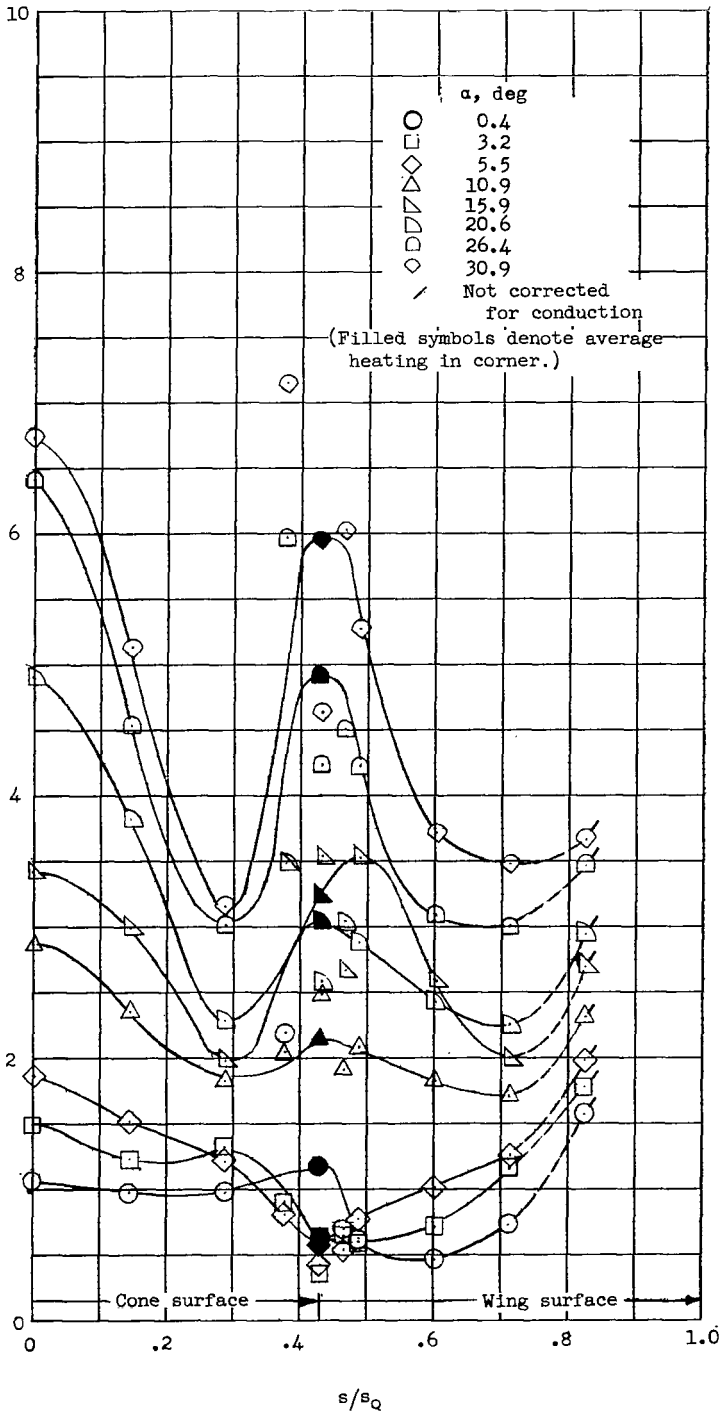

(b) $R_x = 0.5 \times 10^6$.

Figure 8.- Concluded.

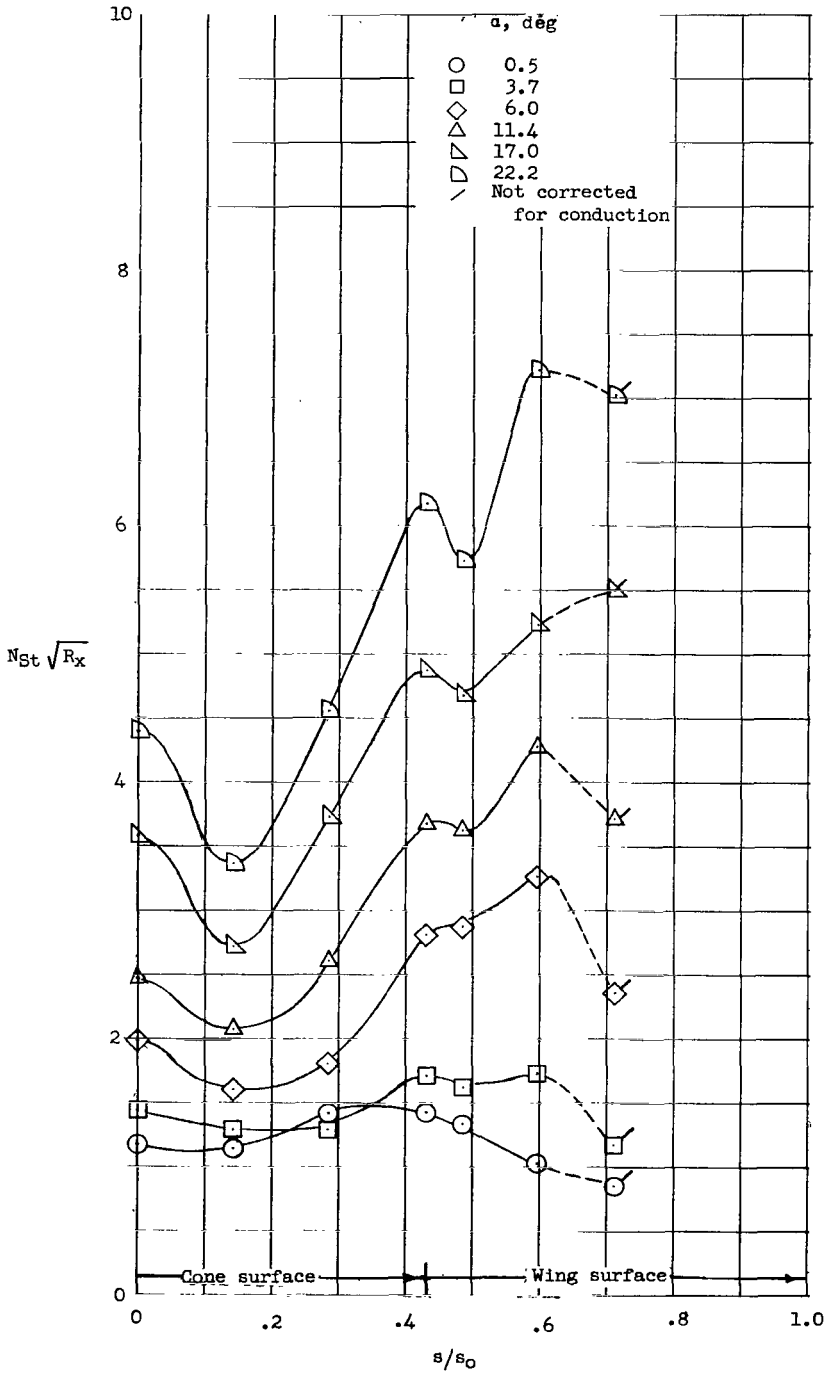

(a) $R_x = 1.5 \times 10^6$.

Figure 9.- Spanwise heating distribution on a delta-wing—half-cone configuration at $M = 6.8$ and $R_c = 3.1 \times 10^6$.

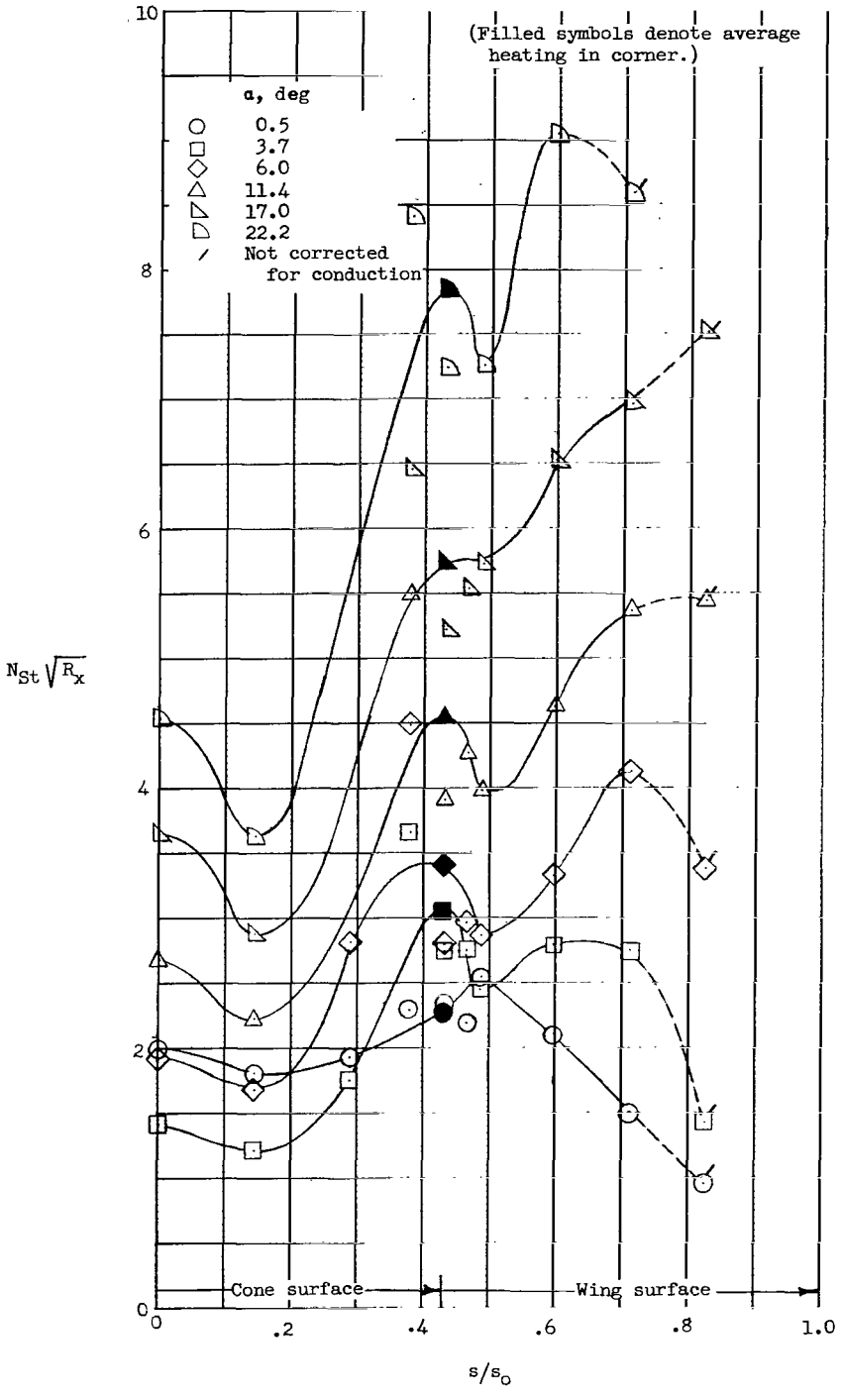

(b) $R_x = 2.8 \times 10^6$.

Figure 9.- Concluded.

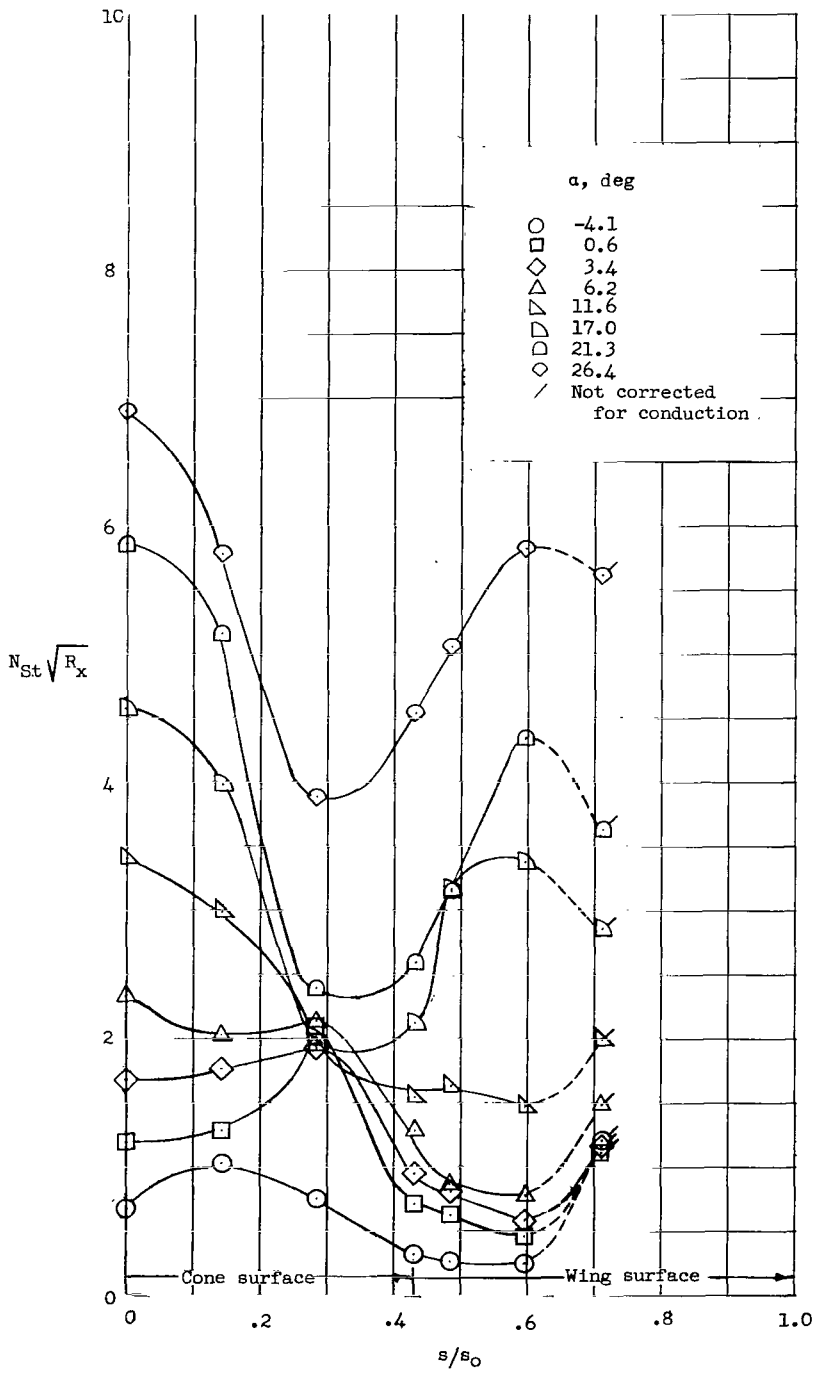

(a) $R_x = 0.5 \times 10^6$.

Figure 10.- Spanwise heating distribution on a delta-wing—half-cone configuration at $M = 9.6$ and $R_c = 1.1 \times 10^6$.

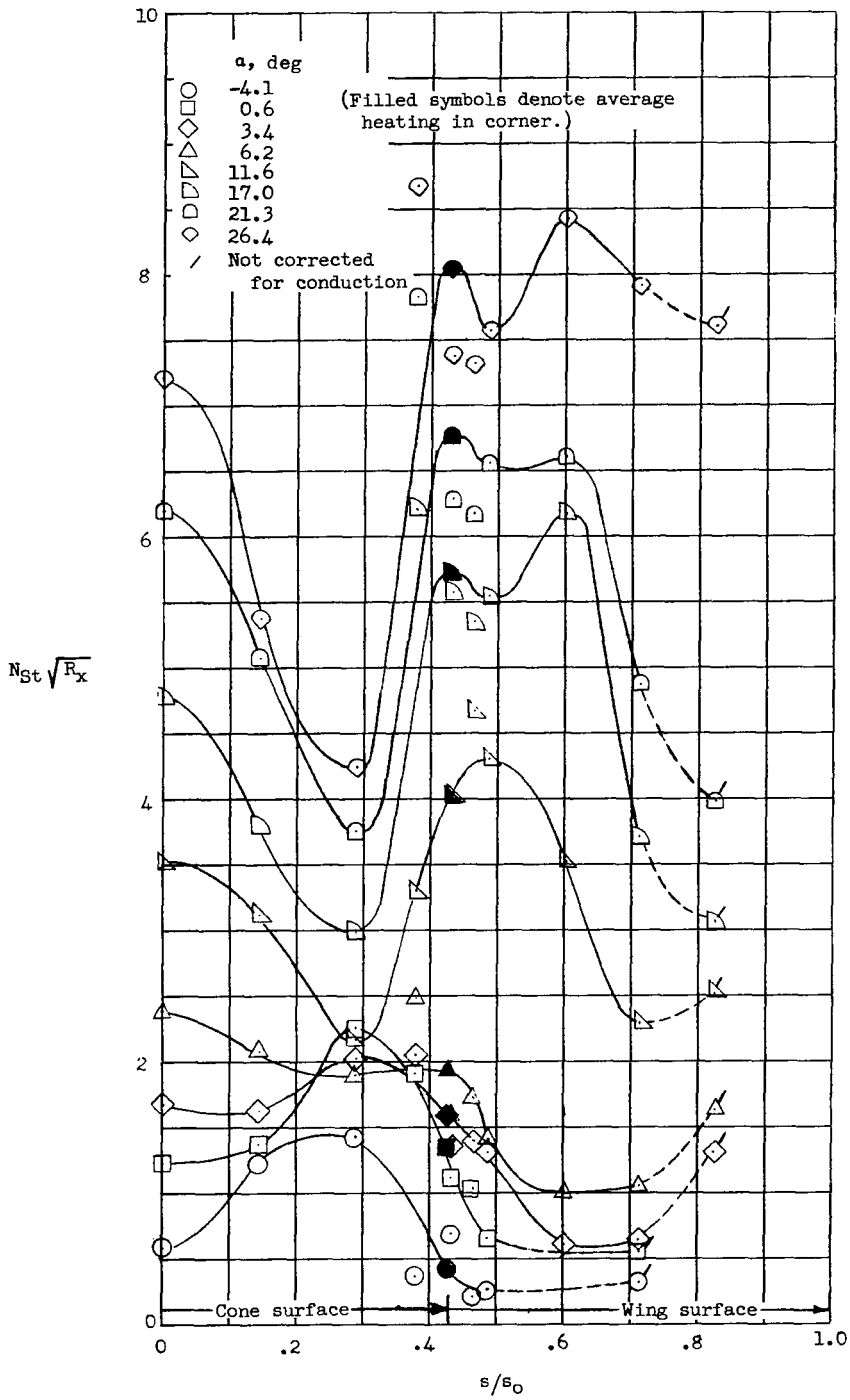

(b) $R_x = 1.0 \times 10^6$.

Figure 10.- Concluded.

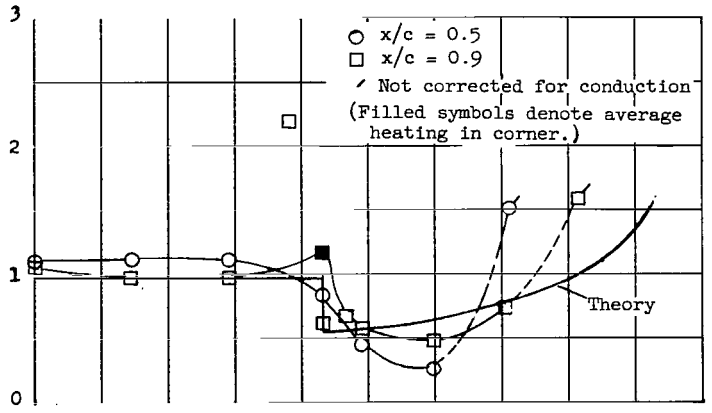

(a) $M = 6.6$; $R_c = 0.6 \times 10^6$; $\alpha = 0.4^\circ$.

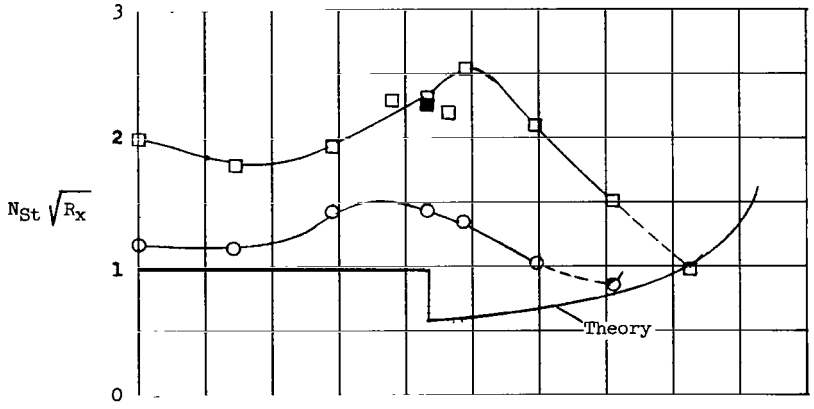

(b) $M = 6.8$; $R_c = 3.1 \times 10^6$; $\alpha = 0.5^\circ$.

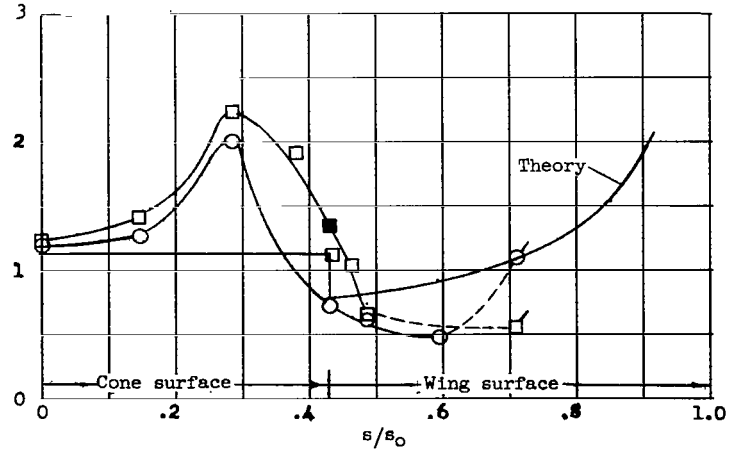

(c) $M = 9.6$; $R_c = 1.1 \times 10^6$; $\alpha = 0.6^\circ$.

Figure 11.- Comparison of distribution of heat-transfer correlating parameter at $\alpha \approx 0^\circ$ with that calculated from laminar strip theory.

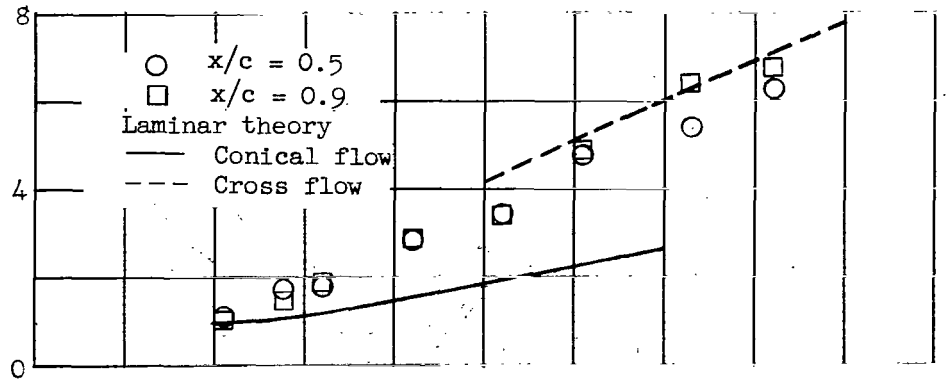

(a) M = 6.6; $R_c = 0.6 \times 10^6$.

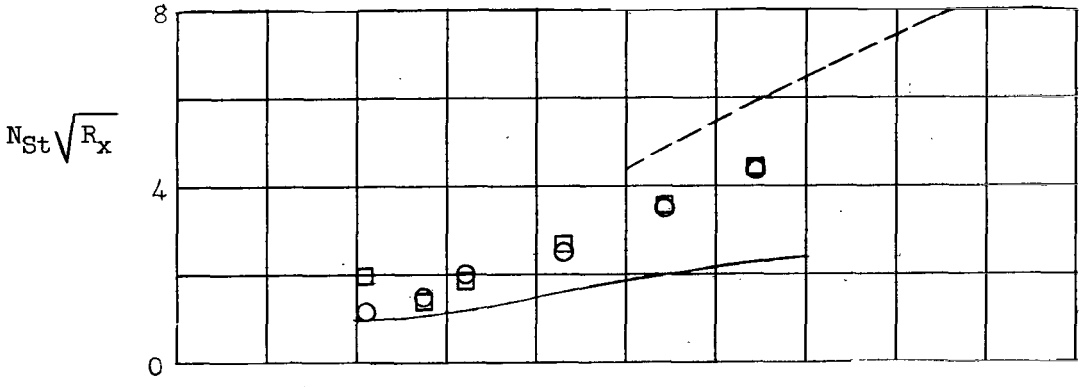

(b) M = 6.8; $R_c = 3.1 \times 10^6$.

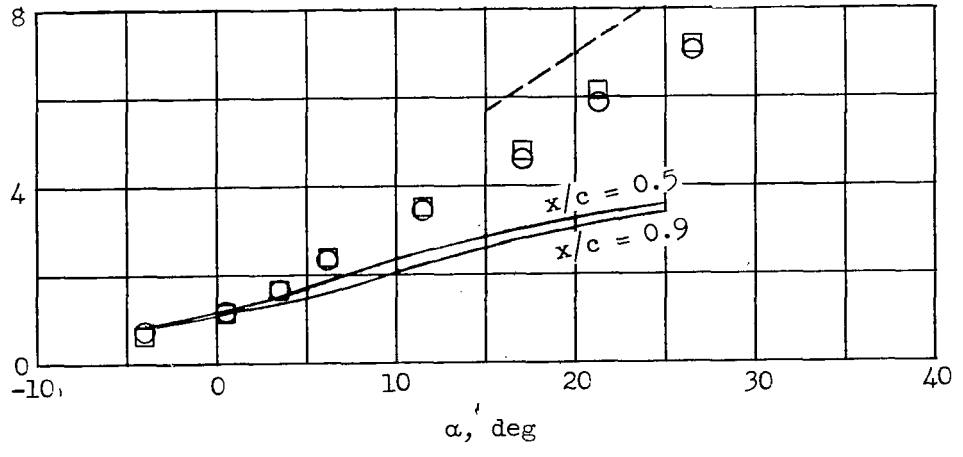

(c) M = 9.6; $R_c = 1.1 \times 10^6$.

Figure 12.- Comparison of heat-transfer correlating parameter measured on stagnation line of cone ($s/s_o = 0$) with that calculated from laminar theory in which measured pressures are used.

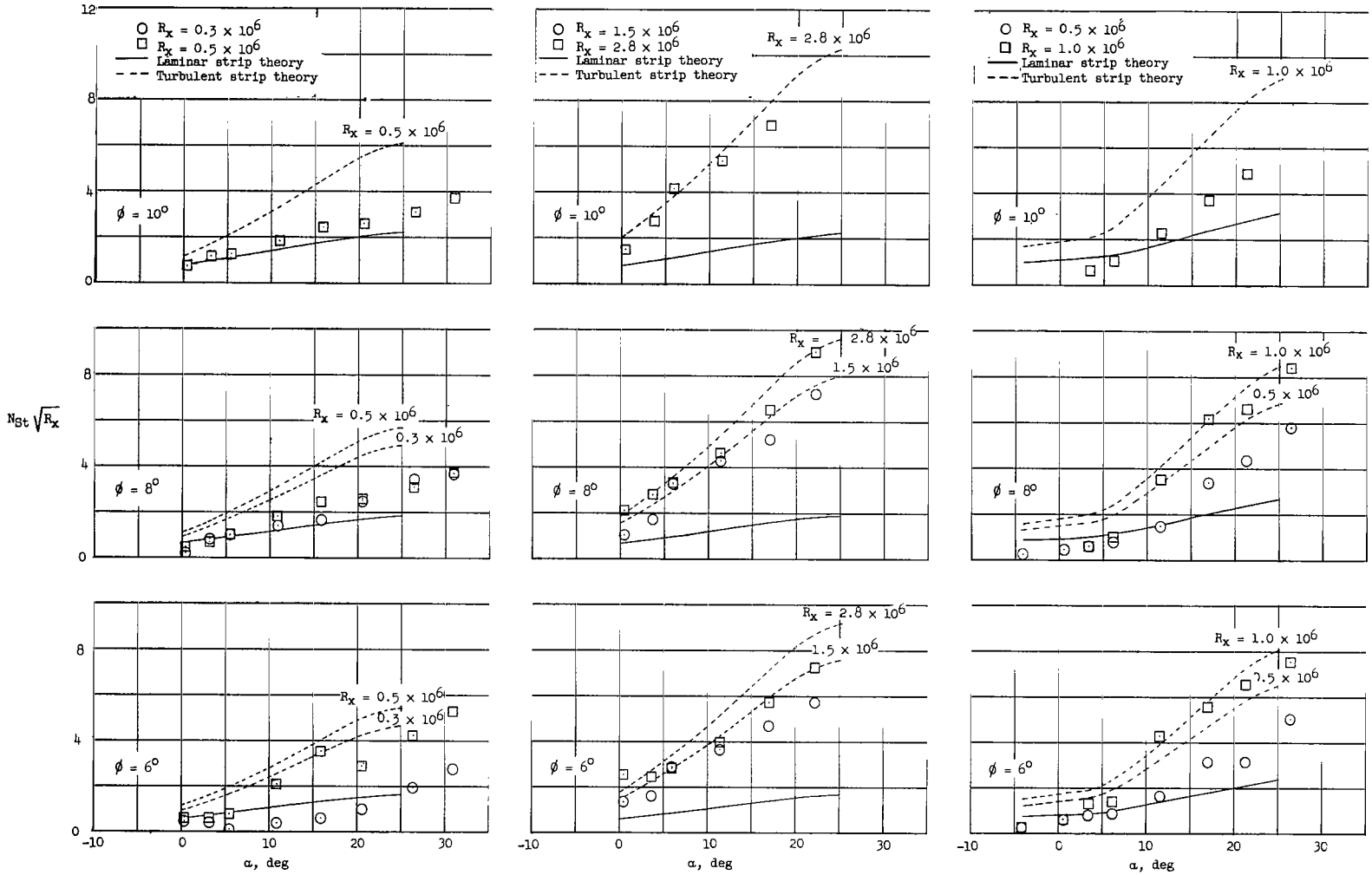

(a) M = 6.6 (b) M = 6.8. (c) M = 9.6.

Figure 13.- Comparison of laminar heat-transfer correlating parameter with that calculated from turbulent and strip theories for wing-surface rays.